Enolpyruvyl Activation by Enolpyruvylshikimate-3-phosphate Synthase†

Meghann E. Clark‡,|| and Paul J. Berti*,‡,§,||

Departments of Chemistry and Biochemistry and Biomedical Sciences and Antimicrobial Research Centre, McMaster University, Hamilton, Ontario L8S 4M1, Canada

Received September 1, 2006; Revised Manuscript Received December 12, 2006

ABSTRACT: Enolpyruvylshikimate-3-phosphate synthase (AroA, also called EPSP synthase) is a carboxyvinyl transferase involved in aromatic amino acid biosynthesis, forming EPSP from shikimate 3-phosphate and phosphoenolpyruvate. Upon extended incubation, EPSP ketal, a side product, forms by intramolecular nucleophilic addition of O4 to C2′ of the enolpyruvyl group. The catalytic significance of this reaction was unclear, as it was initially proposed to arise from nonenzymatic breakdown of tetrahedral intermediate that had dissociated from AroA. This study shows that EPSP ketal formed in AroA's active site, not nonenzymatically, by demonstrating its formation in the presence of excess AroA. It formed both in the normal reaction and during AroA-catalyzed EPSP hydrolysis. In addition, nonenzymatic EPSP hydrolysis was studied to elucidate the catalytic imperative for enolpyruvyl reactions. Hydrolysis was acid-catalyzed, with a rate enhancement of $>5 \times 10^8$-fold. There was no detectable EPSP breakdown after 16 days at 90 °C in 1 M KOH, a solution that is 1000-fold more nucleophilic than neutral aqueous solutions. Thus, an unactivated enolpyruvyl group is not susceptible to nucleophilic attack. Enzymatic EPSP ketal formation therefore requires enolpyruvyl activation through protonation of C3′ to form either a cationic intermediate or a highly cation-like transition state. Forming an EPSP cation requires the investment of considerable catalytic power by AroA. Such an intermediate is a potential target motif for inhibitor design.

Although the overall reaction pathway and kinetic mechanism of the carboxyvinyl transferase enolpyruvylshikimate-3-phosphate synthase (AroA, also called EPSP synthase) has been well characterized (*1*), the catalytic imperative of the individual steps is not well understood. AroA forms enolpyruvylshikimate 3-phosphate (EPSP)[1] from shikimate 3-phosphate (S3P) and phosphoenolpyruvate (PEP) (Figure 1). This is part of the shikimate pathway of aromatic compound biosynthesis in bacteria, plants, and some parasites (*1*, *2*). The plant homologue is targeted by glyphosate [*N*-(phosphonomethyl)glycine], a herbicide (*3*). MurA, its only homologue, also a carboxyvinyl transferase, is part of the peptidoglycan biosynthesis pathway in bacteria and is the target of fosfomycin, an antibiotic (*4*).

AroA and MurA catalyze addition−elimination reactions proceeding through tetrahedral intermediates (THI). Important mechanistic questions remain; even the identity of the catalytic residues is controversial (*5*−*7*). Some evidence points to cationic intermediates in the AroA reaction: Solvent deuterium exchange in PEP in the presence of the substrate analogue 4,5-dideoxyshikimate 3-phosphate indicates PEP cation formation (*1*, *8*). Glyphosate was long considered a mimic of a cation intermediate (*8*, *9*). However, the fact that it is an uncompetitive inhibitor against EPSP suggests that glyphosate does not bind in the same physical space as the enolpyruvyl moiety (*10*, *11*). EPSP ketal (EPSPK) formation could be taken as evidence for an EPSP cation intermediate; however, it was originally proposed to arise from nonenzymatic breakdown of THI which had dissociated from the enzyme (*12*). Because EPSPK formation always occurred in reactions with substrates in excess over AroA (*12*−*15*), a nonenzymatic source was possible. We showed that some EPSPK was formed in nonenzymatic THI breakdown, but too little to account for the amounts in enzymatic reactions (*16*). Others have argued that it forms in the active site but that its slow formation implied an uncatalyzed reaction (*1*).

In order to understand the catalytic imperative of the enzymatic reaction, it is important to understand the inherent reactivity of the enolpyruvyl group. Enol ether breakdown is acid-catalyzed (*17*−*20*), and they are generally base stable (*21*). Acid-catalyzed EPSP hydrolysis was studied under acidic conditions (*22*), but it is not known whether the reaction was also acid-catalyzed at pH >5, nor was it possible to set a limit on the effectiveness of acid catalysis. By studying EPSP breakdown at 90 °C, we show that the reaction is acid-catalyzed beyond pH 10, and it is not susceptible to uncatalyzed nucleophilic attack, even in 1 M KOH (pH 14).

† This work was supported by the Canadian Institutes of Health Research.

* Author to whom correspondence should be addressed. Telephone: (905) 525-9140 ext 23479. Fax: (905) 522-2509. E-mail: berti@mcmaster.ca.

‡ Department of Biochemistry and Biomedical Sciences, McMaster University.

§ Department of Chemistry, McMaster University.

|| Antimicrobial Research Centre, McMaster University.

[1] Abbreviations: AroA, EPSP synthase; CAPS, potassium 3-(cyclohexylamino)propane-1-sulfonate; EPSP, enolpyruvylshikimate 3-phosphate; EPSPK, EPSP ketal; HEPES, potassium 4-(2-hydroxyethyl)-1-piperazineethanesulfonate; MES, potassium 2-morpholin-4-ylethanesulfonate; MurA, UDP-GlcNAc enolpyruvyl transferase; PEP, phosphoenolpyruvate; P_i, inorganic phosphate; S3P, shikimate 3-phosphate; SDKIE; solvent deuterium kinetic isotope effect; THI, tetrahedral intermediate.

10.1021/bi0618316 CCC: $37.00
Published on Web 01/27/2007

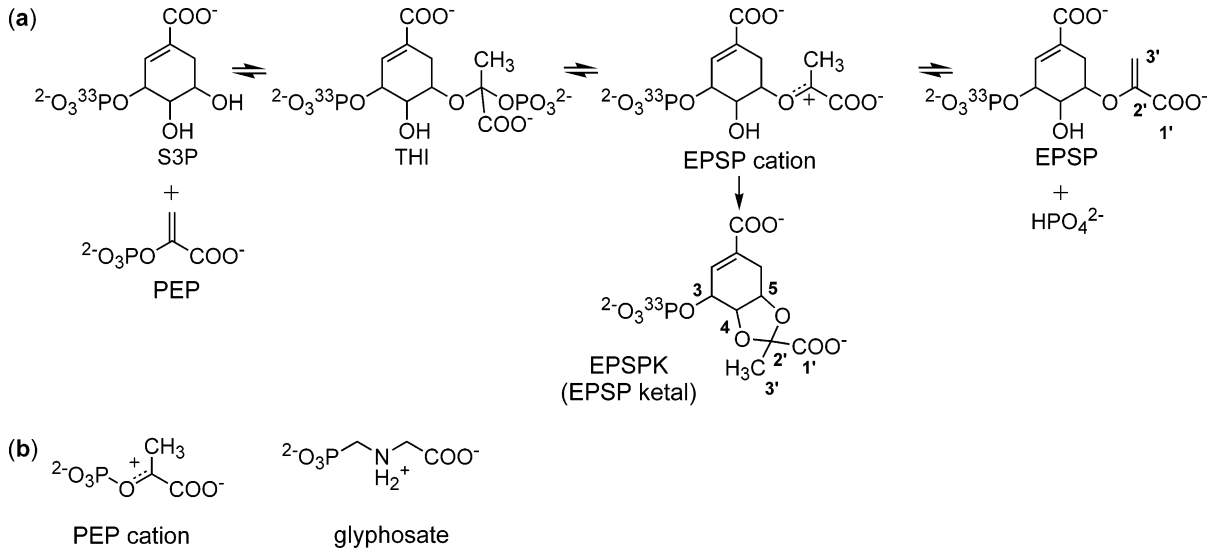

FIGURE 1: (a) Catalytic mechanism of AroA, including the putative EPSP cation. (b) PEP cation and the AroA inhibitor, glyphosate.

Enolpyruvyl cations are very unstable and would require >15 kcal/mol to form based on their pK_a's and solvent deuterium kinetic isotope effects of hydrolysis (*17*, *22*). Catalyzing their formation would represent a major investment of an enzyme's catalytic power.

In this study, we have demonstrated that EPSPK forms in the presence of excess AroA, eliminating nonenzymatic THI breakdown as the source. Significant amounts of EPSPK formed during AroA-catalyzed EPSP hydrolysis, demonstrating that this is not a rare catalytic mistake. The pH dependence of nonenzymatic EPSP breakdown showed that acid catalysis accelerated hydrolysis $>5 \times 10^8$-fold and that it is not susceptible to nucleophile catalysis. This implies that AroA must promote EPSP breakdown through enolpyruvyl activation, forming either the EPSP cation or a highly cation-like transition state.

MATERIALS AND METHODS

General. Unless specified, all reagents were from Sigma/Aldrich or Bioshop Canada (Burlington, Ontario, Canada). [γ-^{33}P]ATP was from GE Healthcare. *Escherichia coli* AroA containing a C-terminal His_6 tag was prepared as described previously (*5*). The active AroA concentration was determined by fluorescence titration of 0.5 μM AroA with S3P in the presence of 250 μM glyphosate (*5*, *11*, *23*). Typically, active AroA was ~45% of the total protein concentration, consistent with our previous findings (*5*) and a previous report where glyphosate binding to AroA·EPSP had a stoichiometry of ~63% (*11*). Shikimate 3-phosphate (S3P) and [^{33}P]S3P were prepared as described previously but using [γ-^{33}P]ATP (*5*). Purification was by anion-exchange chromatography (Mono Q, 5 × 50 mm; GE Healthcare) with a gradient of 50−800 mM ammonium formate, pH 8, over 30 min, 0.5 mL/min, and A_{240} detection. [^{33}P]EPSP was prepared from [^{33}P]S3P in a 1 mL reaction containing 50 mM Tris-HCl, pH 7.5, 0.5 μM AroA, 150 μM [^{33}P]S3P, and 300 μM PEP. Purification was by anion-exchange chromatography (Mono Q) with a gradient of 100−600 mM ammonium bicarbonate, pH 10, over 30 min at 0.5 mL/min and A_{240} detection.

EPSP Ketal Formation with Excess AroA. Reactions to detect EPSPK contained 600 or 750 μM [^{33}P]S3P (0.7 or 0.9 μCi), 1.33 equiv of active AroA (800 or 1000 μM), and either equimolar or 6.7 equiv of PEP in 100−250 μL of 50 mM potassium HEPES, pH 7.0, 50 mM KCl, and 5% glycerol, at 25 °C. Some reactions with excess PEP also contained 10 mM potassium phosphate (P_i). Aliquots of the reaction were quenched with 0.2 M KOH, and protein was removed by centrifugal ultrafiltration over 10 kDa cutoff membranes (Microcon YM10; Millipore Corp.). The reaction products were then separated by ion-paired C18 reverse-phase HPLC (4.6 × 250 mm, Supelcosil LC-18-T, 5 μm particles) with isocratic elution in 100 mM potassium phosphate, pH 6.0, and 4 mM $(Bu_4N^+)_2SO_4^{2-}$ at 1 mL/min. ^{33}P was detected by flow scintillation analysis using an in-line flow scintillation analyzer, with Ultima-Flo AP (Packard) scintillation fluid mixed with the column eluate at 4 mL/min. The approximate elution times were as follows: [^{33}P]-S3P, 9.6 min; [^{33}P]EPSPK, 22.5 min; [^{33}P]EPSP, 33.9 min. No [^{33}P]THI was observed in any experiment. We showed previously that 0.2 M KOH does not completely denature $AroA_{H6}$·THI (*5*). Over the time required to remove the protein by ultrafiltration, [^{33}P]THI was converted enzymatically to [^{33}P]S3P and [^{33}P]EPSP. Concentrations of [^{33}P]S3P, [^{33}P]EPSPK, and [^{33}P]EPSP were calculated from the ratios of peak areas from flow scintillation analysis and the known [^{33}P]S3P concentration at the beginning of the reaction or [^{33}P]EPSP for hydrolysis reactions.

Unlabeled EPSPK for NMR identification was prepared under the same conditions from a 10 mL reaction mixture.

EPSP-Only Reactions. AroA-catalyzed [^{33}P]EPSP breakdown reactions were conducted with the same conditions and methods as above, with 750 μM [^{33}P]EPSP (0.5 μCi) and 1000 μM active AroA in 100 μL of 50 mM potassium HEPES, pH 7.0, 50 mM KCl, and 5% glycerol, at 25 °C.

Nonenzymatic EPSP Hydrolysis. Nonenzymatic EPSP hydrolyses where the reaction proceeded to near completion in 1 day were followed by reduction of the product pyruvate with lactate dehydrogenase. The concomitant oxidation of NADH to NAD^+ was detected by A_{340}, with $\epsilon_{340} = 6220$ M^{-1} cm^{-1} (*24*). Aliquots (100 μL) of the EPSP hydrolysis mixture were reacted with 700 μL of 50 mM Tris-HCl, pH 7.5, 50 μM KCl, 50 μM $MgCl_2$, 10 units/mL LDH, and 200 μM NADH in a quartz cuvette, and the ΔA_{340} was measured.

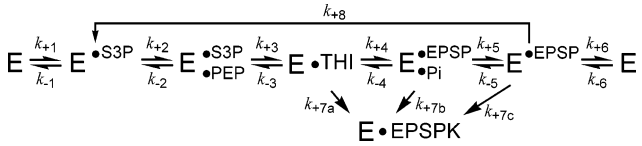

FIGURE 2: AroA kinetic mechanism. Except for k_{+7} and k_{+8}, rate constants were from ref *1*. Key: E, AroA, P_i, phosphate. The center dot indicates a noncovalent complex. The second product of step k_{+8} is pyruvate. For EPSP hydrolysis, only rate constants $k_{\pm 6}$, k_{+7c}, and k_{+8} are relevant.

Multiday high-pH reactions with small extents of reaction were followed by ion-exchange chromatography. Each 100 μL reaction aliquot was diluted to 500 μL with 100 mM ammonium bicarbonate, pH 10, injected on an anion-exchange column (Mono Q), and eluted with a gradient of 100−700 mM ammonium bicarbonate, pH 10, over 36 min at 0.5 mL/min, with A_{240} detection. EPSP was quantified relative to S3P with relative molar absorptivities of $\epsilon_{S3P}/\epsilon_{EPSP} = 0.28$ (*25*). To minimize evaporation, reaction mixtures were overlaid with mineral oil and incubated in a thermocycler with a heated lid.

All reactions contained 500 μM EPSP and were run at 90 °C in 50 mM buffer. The buffers used were sodium acetate (pH 4−6), MES (pH 4.9−6.9), HEPES (pH 7.2−8.2), CAPS (pH 8.6−9.7), potassium phosphate (pH 2, 2.9, and 11.3), and 1 M KOH for the pH 14 reaction. The pK_a's of most of the buffers were temperature dependent, so pHs were measured at 90 °C.

Rates at each pH were determined by fitting to linear or first-order rate equations, depending on the extent of reaction. The pH dependence was fitted to a two pK_a model with the rate going to zero at high pH as there was no evidence of a pH-independent rate at high pH (eq 1):

$$k_{\text{hydrolysis}} = \frac{k_A \times 10^{-pH}}{1 + 10^{-(pK_1 - pH)} + 10^{-(pK_1 + pK_2 - 2pH)}} + \frac{k_B \times 10^{-pH}}{10^{-(pH - pK_1)} + 1 + 10^{-(pK_2 - pH)}} + \frac{k_C \times 10^{-pH}}{10^{-(2pH - pK_1 - pK_2)} + 10^{-(pH - pK_2)} + 1} \quad (1)$$

where $k_{\text{hydrolysis}}$ is the first-order rate constant at a given pH and k_A, k_B, and k_C are the second-order rate constants for different protonation states of EPSP (see Figure 3b).

Data Analysis for EPSP Ketal Formation. The rates of formation/disappearance of EPSPK, S3P, and EPSP were analyzed by numerical simulation and by fitting to first-order rate constants. Numerical simulations used the AroA kinetic mechanism elucidated by Anderson and Johnson (*26*, *27*) under the same reaction conditions, except for the presence of 5% glycerol in the present study (Figure 2). This equilibrium-ordered mechanism is somewhat incorrect in that more recent kinetic investigations support a random kinetic mechanism (*28*, *29*); however, using the exact mechanism would have no effect on the fitted rate constants. Formation of the E·EPSPK complex was treated as being irreversible. Given the tight binding, $K_d = 3$ μM (*13*), and large excess of free AroA in the reaction mixture, this approximation would have no effect on the kinetics.

Simulations were performed using KinTekSim, an implementation of KinSim and FitSim (*30*, *31*). The microscopic rate constants k_{+1} to k_{-6} were fixed at the previously reported values (*26*, *27*), and the values of k_{+7a-c} and k_{+8} were fitted. As there was no evidence to support rate constants k_{+7a-c} being different from each other (see below), they were eventually made equal. Significant amounts of E·[^{33}P]THI exist in the reaction mixtures (see Supporting Information), but no [^{33}P]THI was observed because 0.2 M KOH does not denature $AroA_{H6}$·THI (*5*), which is converted instead to [^{33}P]S3P and [^{33}P]EPSP. Partitioning E·[^{33}P]THI in the numerical simulations 41% to [^{33}P]S3P and 59% to [^{33}P]-EPSP gave the best match to experimental data at early reaction times, before significant [^{33}P]EPSPK had formed.

Nonlinear least-squares fitting to first-order rate constants would be expected to be appropriate for some reactions, namely, {excess PEP + 10 mM P_i} or EPSP only (eqs 2 and 3).

$$[\text{EPSPK}]_i = [\text{EPSPK}]_\infty(1 - \exp(-k_{+7}t)) \quad (2)$$

$$[\text{S3P}]_i = \{([\text{S3P}]_\infty - [\text{S3P}]_0)(1 - \exp(-k_{+8}t))\} + [\text{S3P}]_0 \quad (3)$$

The rate constants for EPSP disappearance were within experimental error of ($k_{+7} + k_{+8}$), as expected, and are not reported separately.

Reactions containing excess PEP but no added P_i or PEP equimolar with S3P would not necessarily be expected to fit to eqs 2 and 3 because the proportions of species potentially able to form EPSPK, such as E·EPSP·P_i, would change through the course of the reaction. If, for example, $k_{+7b} > k_{+7c}$, EPSPK formation would accelerate as P_i accumulated, while it would slow if $k_{+7c} > k_{+7b}$. These reactions fit well to eqs 2 and 3, which implies that the values of k_{+7a} to k_{+7c} were broadly similar, though it is not known how sensitive the progress curves would be to differences in the values of k_{+7a} to k_{+7c}.

RESULTS

Our initial observation that EPSPK formed in reactions with excess AroA demonstrated that it formed in the active site, rather than through THI dissociation. In order to better understand this reaction, enzymatic EPSPK formation and EPSP hydrolysis were characterized in detail. In addition, nonenzymatic EPSP hydrolysis was studied in order to probe the limits of acid catalysis and to determine whether uncatalyzed nucleophilic attack on the enolpyruvyl group was possible.

Acid-Catalyzed EPSP Hydrolysis. Kresge et al. studied acid-catalyzed EPSP hydrolysis at 25 °C from 60% $HClO_4$ to pH 4.8 (*22*). We extended the pH profile to pH 14 by running reactions at 90 °C and fitting the data to eq 1 (Figure 3). The highest second-order rate constant was for the fully deprotonated form of EPSP (C in Figure 3b), $k_C = 520$ M^{-1} s^{-1}, indicating that the four negative charges helped to electrostatically stabilize the EPSP cation. 3-Phosphate protonation, with p$K_2 = 6.5$, decreased electrostatic stabilization of the EPSP cation, leading to a 12-fold decrease in the second-order rate constant, $k_B = 45$ M^{-1} s^{-1}. pK_1 was 3.9 ± 0.5, within experimental error of the literature value, 3.77 (*22*), and was attributed to the C1′ carboxyl. This caused a

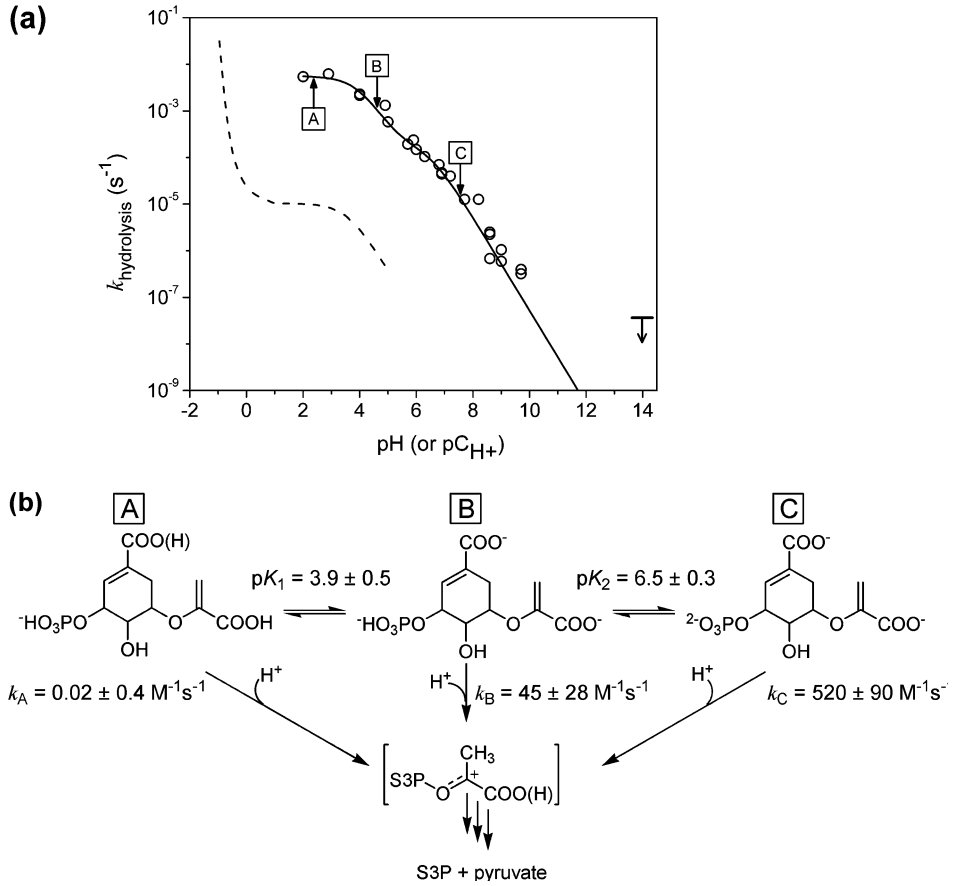

FIGURE 3: (a) pH (or pC_{H^+}) dependence of nonenzymatic EPSP hydrolysis. (○, —) EPSP hydrolysis at 90 °C (this study). The bar at pH 14 represents the upper limit of the experimental rate. The curve shows the best fit to eq 1. (- - -) EPSP breakdown at 25 °C, fitted to eqs 4 and 10 of ref *22*. The steep pH dependence at pH <0 reflects the excess acidity of concentrated $HClO_4$ solutions (*32*), which behave as though they were more acidic than expected from $[H^+]$. (b) EPSP structures A−C correspond to the dominant EPSP protonation state at the indicated pHs. The second-order rate constants, k_A−k_C, for acid-catalyzed hydrolysis are shown.

large decrease in the second-order rate constant to $k_A = 0.02 \pm 0.4$ M^{-1} s^{-1}. The standard error was larger than the fitted value, reflecting the fact that (1) the value of k_A is poorly defined in the plateau region and (2) k_A was not constrained to be greater than zero. (Negative rate constants are mathematically possible in eq 1 but physically meaningless.) k_A would be well-defined only if there were experimental data in the pH-dependent region below pH 1, but it was nonetheless clearly much less than k_B. Fitting the data to eq 1 while fixing $k_A = 0$ changed the other fitted parameters by <3%. The protonation state of the distal carboxyl at C1 did not have a visible effect on the reaction rate, though its pK_a is presumably similar to C1′.

At pH 2 and 90 °C, $k_{hydrolysis} = 5.5 \times 10^{-3}$ s^{-1}, while the corresponding value at 25 °C was $k'_{H^+}Q_a = 1.04 \times 10^{-5}$ s^{-1} (*22*). Thus, the temperature difference caused a 532-fold difference in rate constants.

There was no detectable EPSP hydrolysis after 11 days at pH 11.3 or 16 days at pH 14. Assuming that 5% breakdown could have been detected, the upper limit of the rate at pH 14 would be 4×10^{-8} s^{-1} at 90 °C or 7×10^{-11} s^{-1} if converted to 25 °C. EPSPK was not observed in any nonenzymatic reaction. Given the generally low stability of ketals with bulky substituents (*33*, *34*), it would likely break down faster than it formed, and so no significance was assigned its absence.

Enzymatic EPSP Ketal Formation. (A) AroA Reaction Products. Reaction mixtures contained 800 or 1000 μM active AroA, in 25% excess over [^{33}P]S3P (600 or 750 μM). Given THI's 8 min solution lifetime under the reaction conditions (*16*) and the fact that THI reacts with AroA at an almost diffusion-controlled rate, $k_{cat}/K_M = 10^8$ M^{-1} s^{-1} (*5*, *27*), any released THI would rebind faster than it broke down.[2] EPSPK was formed under these conditions. Its identity was confirmed by comparison with the previously reported NMR chemical shifts (*12*) and comparison with the S3P and shikimic acid spectra (see Supporting Information).

In reactions containing equimolar [^{33}P]S3P and PEP, [^{33}P]-EPSPK was 18% of the final products, with the remainder being [^{33}P]S3P that arose from [^{33}P]EPSP and/or PEP hydrolysis (Figures 2 and 4). With PEP present in excess over [^{33}P]S3P, the yield of [^{33}P]EPSPK was >95% with or without 10 mM P_i. [^{33}P]S3P formed by [^{33}P]EPSP hydrolysis could react with the excess PEP and reenter the equilibrium. [^{33}P]EPSPK also formed 8% of the [^{33}P]EPSP hydrolysis products. This demonstrated conclusively that [^{33}P]EPSPK formed in the AroA active site during the normal reaction, as well as during [^{33}P]EPSP hydrolysis.

AroA has been reported to bind EPSPK with $K_d = 3$ μM (*13*). As observed previously (*12*), excess AroA did not appreciably hydrolyze [^{33}P]EPSPK under these reaction

[2] Assuming that $K_{d,THI} = 1$ nM [estimated $K_{d,THI} = 50-260$ pM (*27*, *35*)], the equilibrium concentration of free THI would be 750 pM, and the fraction of EPSPK arising nonenzymatically would be 0.0004% of the total.

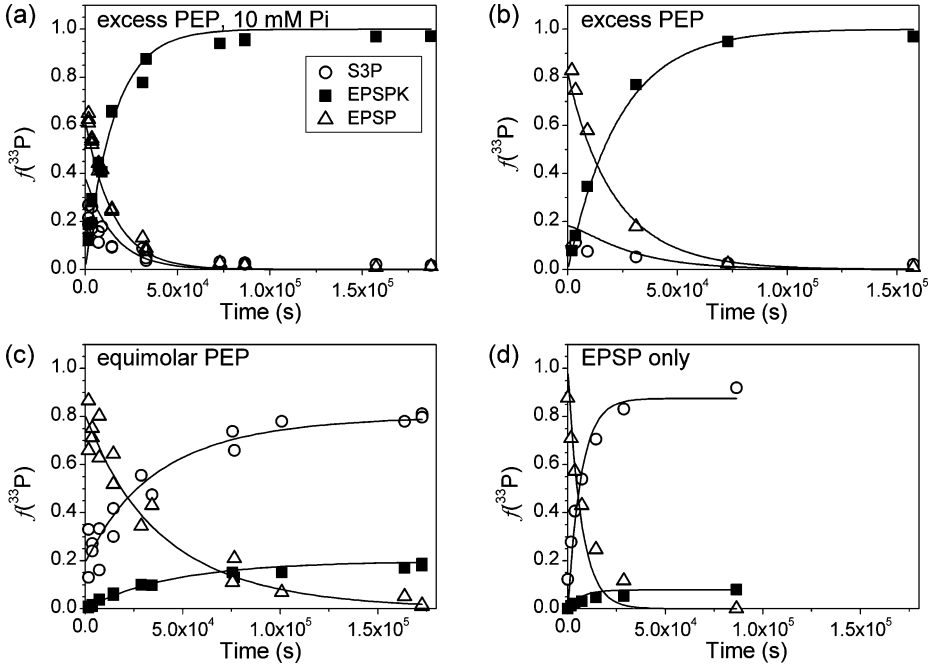

FIGURE 4: Reaction profiles for EPSP ketal formation under different conditions. $f(^{33}P)$ is the fraction of total ^{33}P for each species. Panels: (a) excess PEP + 10 mM P_i (S3P:PEP:AroA = 1:6.7:1.33); (b) excess PEP (S3P:PEP:AroA = 1:6.7:1.33); (c) equimolar PEP and S3P (S3P:PEP:AroA = 1:1:1.33); (d) no PEP (EPSP:AroA = 1:1.33). The solid lines were calculated using the rate constants from the numerical simulations (Table 1) and from ref *1*.

Table 1: Rates of [^{33}P]EPSPK Formation and [^{33}P]EPSP Hydrolysis[a]

	first-order fit[b]		numerical simulation		
conditions	k_{+7} (s^{-1})[c]	k_{+8} (s^{-1})[c]	k_{+7} (s^{-1})[d]	k_{+8} (s^{-1})[d]	n[e]
6.7 equiv of PEP + 10 mM P_i	8.0 (±0.5) × 10^{-5}		5 (±1) × 10^{-5}	nd[f]	3
6.7 equiv of PEP	4.9 (±0.1) × 10^{-5}		4.3 × 10^{-5}	nd[f]	1
1 equiv of PEP	4.5 (±0.4) × 10^{-6}	1.8 (±0.4) × 10^{-5}	5 (±2) × 10^{-6}	4 (±2) × 10^{-5}	2
[^{33}P]EPSP	1.2 (±0.1) × 10^{-5}	1.3 (±0.3) × 10^{-4}	1.1 × 10^{-5}	1.1 × 10^{-4}	1

[a] Previously determined rate constants (k_{+1} to k_{-6}) were fixed (*26*, *27*). [b] Fitted to eqs 2 (k_{+7}) and 3 (k_{+8}). [c] Data points from all independent trials were fitted simultaneously (±standard error of fit). [d] Mean (±standard error) of independent trials. [e] Number of independent trials. [f] Not determined, fixed at the average value from the trials with 1 equiv of PEP.

conditions. After 12 days, 18% had broken down. As ketal hydrolysis has a different catalytic imperative (protonation at O4 or O5 by a general acid catalyst), this reaction was not pursued. No [^{33}P]THI was observed because 0.2 M KOH does not completely denature $AroA_{H6}$•[^{33}P]THI (*5*), which is then converted to [^{33}P]S3P and [^{33}P]EPSP during the ultrafiltration step before chromatographic separation.

(B) Kinetics of EPSP Ketal Formation. [^{33}P]EPSPK formation was analyzed both by numerical simulation and by fitting to first-order rate constants (Table 1).

(C) Numerical Simulations. Numerical simulation is necessary to extract rate constants for reactions that do not (necessarily) follow first-order kinetics (*30*). A set of differential equations describing the kinetic mechanism (Figure 2) are integrated numerically to create a time course for all species in the reaction, and the rate constants k_{+7} and k_{+8} are varied until they match the experimental data. The microscopic rate constants k_{+1} to k_{-6} were reported previously by Anderson and Johnson (*26*, *27*). Our conditions were identical except for the addition of 5% glycerol, which had no measurable effect on the rate (data not shown). Although a His-tagged variant of AroA was used in this study, we previously demonstrated that THI partitioning and specific activity were the same as wild type (*5*), indicating that the internal equilibria were unchanged. $K_{d,EPSP}$ was also unchanged (*25*). The rate of EPSPK formation with excess PEP was (4−8) × 10^{-5} s^{-1}, in good agreement with the literature value of 3.3 × 10^{-5} s^{-1} (*1*) and in good agreement with the first-order fits (see below).

(D) First-Order Rate Constants. The experimental data fit well to first-order rate equations in the two reaction conditions where it would be expected, namely, [^{33}P]EPSP hydrolysis and {excess PEP + 10 mM P_i}. The proportion of potential [^{33}P]EPSPK precursor species, mainly, E•[^{33}P]-THI and E•[^{33}P]EPSP•P_i, would be constant throughout the reaction and give rise to pseudo-first-order kinetics. The other reaction conditions, namely, equimolar PEP and [^{33}P]S3P and excess PEP without P_i, also fit well to the first-order rate equations and gave similar results to the numerical simulations. This indicates that, within the resolution of the kinetic mechanism (Figure 2), the values of k_{+7a} to k_{+7c} were the same and that the changing proportion of enzyme-bound species as the reaction progressed did not affect the kinetics.

(E) Comparison of Rate Constants. The values of k_{+7} and k_{+8} from first-order rate equations generally agreed well with the numerical simulations (Table 1). The exception was k_{+8} for equimolar [^{33}P]S3P and PEP, which was 2-fold higher in the numerical simulation. However, the error in the value

from the numerical simulation was large. The values of k_{+7} were reproducibly lower for reactions with equimolar PEP than with excess PEP for reasons that are not clear. The rate constants for [^{33}P]EPSP hydrolysis from first-order fits and numerical simulations, k_{+8}, were in excellent agreement with each other, 1.3×10^{-4} s^{-1} and 1.1×10^{-4} s^{-1}, and in reasonable agreement with the previously reported value, 5×10^{-4} s^{-1} (*26*). The high AroA concentration, which was close to saturation, may have had some effect on its activity, as the EPSP hydrolysis rate was 7×10^{-4} s^{-1} with 5−50 μM AroA at pH 7.5 in the presence of a phosphate scavenging system, namely, sucrose phosphorylase, phosphoglucomutase, and glucose-6-phosphate dehydrogenase (data not shown). The fact that hydrolysis was not slowed after phosphate scavenging demonstrated that EPSP hydrolysis was not an artifact of contaminating phosphate and that AroA can stabilize the EPSP cation on its own.

DISCUSSION

Acid-Catalyzed EPSP Hydrolysis. EPSP hydrolysis was acid-catalyzed, which implicates an EPSP cation intermediate in the reaction. This is consistent with nonenzymatic breakdown of the AroA and MurA THIs, which proceeded through an EPSP cation, albeit as part of an ion pair complex with phosphate (*16*). Formally, it is possible that a discrete EPSP cation intermediate is not formed but rather that nucleophilic attack at C2′ begins before C3′ is fully protonated, in a concerted addition step. Given the fact that an unactivated enolpyruvyl group is not susceptible to nucleophilic attack (see below), it is clear that C3′ protonation would have to be greatly advanced over C2′ attack and that the enolpyruvyl group would bear almost a full positive charge at the transition state. In any case, factors affecting EPSP cation stability will also be valid for a concerted but highly cationic transition state.

EPSP was most reactive in its fully deprotonated form, with $k_C = 520$ M^{-1} s^{-1} (Figure 3). 3-Phosphate protonation, with p$K_2 = 6.5$, decreased through-space electrostatic stabilization of the cation at C2′, as reflected by $k_C/k_B = 12$. C1′ protonation changed the strongly electron donating carboxylate ($\sigma_I = -0.2$) to a moderately electron withdrawing carboxylic acid ($\sigma_I = 0.4$) (*36*), inductively destabilizing the EPSP cation. This further decreased the rate by $k_B/k_A = 2000$. Although the error range for k_A was large, the k_B/k_A ratio was consistent with other evidence. The width of the plateau between pH 0.5 and pH 3.5 in the 25 °C data (*22*) implies an ∼1000-fold effect on EPSP cation stability. This, in turn, is consistent with the difference in the first and second ionization constants of oxalic acid, 3.0 pH units, which reflects the effect of a carboxyl adjacent to the ionizable center (*37*, *38*). The combined effect of 3-phosphate and C1′ carboxyl protonations was a 2×10^4-fold decrease in reactivity.

Plateaus were not observed at either the low or high pH extremes. That is, neither the maximum acid-catalyzed nor the uncatalyzed rate constants are known. This makes it impossible to accurately estimate the effectiveness of acid catalysis on EPSP hydrolysis. Nonetheless, the observed range of $k_{hydrolysis}$ between 60% $HClO_4$ and pH 14 was $>5 \times 10^8$-fold, after correcting for the temperature difference. Thus, the catalytic effect of protonating C3′ of the enolpyruvyl group of EPSP is at least 12 kcal/mol, likely much higher. On the basis of an empirical relationship between solvent deuterium kinetic isotope effects (SDKIEs) and free energy of activation for acid-catalyzed enol ether hydrolyses, the SDKIE of 2.3 for EPSP hydrolysis (*22*) implies a free energy of activation of >20 kcal/mol (*17*).

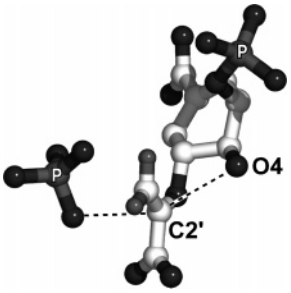

FIGURE 5: EPSP and P_i, showing the positions of the phosphate and O4 nucleophiles relative to C2′. The S3P moiety of this model was superimposed with that from the AroA·S3P·P_i·formate (*40*) and AroA_D313A·THI (*6*) crystal structures, while phosphate was from the AroA·S3P·P_i·formate structure, and the C1′ carboxylate was superimposed with the same atoms in AroA_D313A·THI.

Nucleophile versus Electrophile Activation. (A) Nonenzymatic EPSP Hydrolysis. Can an enolpyruvyl group react with a good nucleophile in the absence of acid catalysis? HO^- is $10^{4.75}$-fold more nucleophilic than H_2O in aqueous solution (*39*). At pH 14 (1 M HO^-), hydroxide is the dominant nucleophile, and the solution is 1000-fold ($=10^{4.75} \times 1$ M $HO^-/55.5$ M H_2O) more nucleophilic than a neutral aqueous solution. EPSP was not hydrolyzed to S3P after 16 days at 90 °C in 1 M KOH, clear evidence against unactivated enolpyruvyl reacting with nucleophiles.

(B) Enzymatic Reactions. This does not completely rule out any sort of nucleophile activation in the enzymatic reaction, but it does show that the effects would be modest and could only occur in conjunction with enolpyruvyl activation. Even if nucleophile activation of P_i does occur in the normal AroA reaction, this is not possible in EPSPK formation because O4, the nucleophile, is located on the opposite side of C2′ from P_i and would be unable to form any of the same contacts with AroA as P_i (Figure 5). Thus, EPSPK formation requires general acid catalysis and activation of the enolpyruvyl group.

Stepwise versus Concerted Reactions. As with the acid-catalyzed reaction, enzymatic enolpyruvyl activation implies a discrete EPSP cation with a finite lifetime in the AroA active site. It is also possible that nucleophilic addition at C2′ occurs when C3′ protonation is advanced, but before the EPSP cation is fully formed, i.e., a concerted addition. Either possibility requires a cationic intermediate or highly cationic transition state.

Is Enolpyruvyl Activation a Rare Event? In the presence of P_i, one turnover in 10^6 leads to EPSPK formation (i.e., k_{cat}/k_{+7}), indicating either that P_i is well poised to attack C2′ or that EPSP cation formation is a rare catalytic mistake. The fact that enzymatic EPSP breakdown yielded 8% EPSPK meant that *at least* 8% of the reaction proceeded through enolpyruvyl activation, and the overwhelming likelihood is that the other 92%, EPSP hydrolysis, did also. The rarity of EPSPK formation is not surprising considering that P_i is well located to attack C2′, while O4 is constrained from close approach by its interactions with Lys340 and Asp313, while

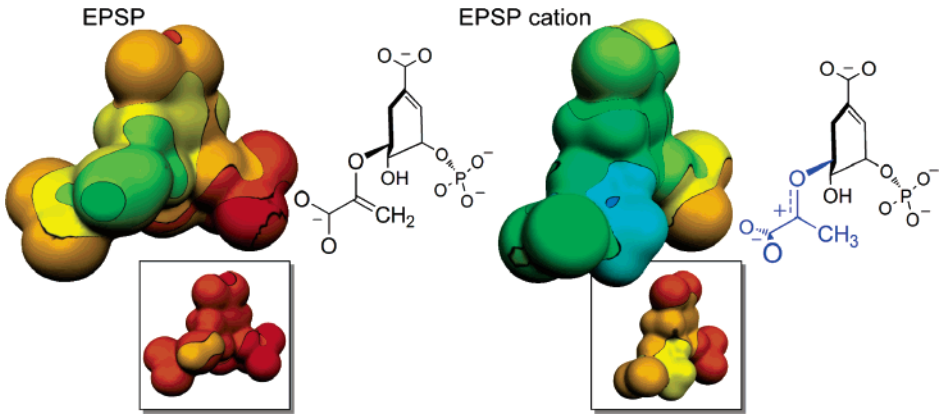

FIGURE 6: Electrostatic potential surfaces of EPSP (left) and the EPSP cation (right) from most negative (red, −0.58 hartree) to least negative (blue, −0.07 hartree). (Inset) Electrostatic potential surfaces plotted from negative (red, −0.58 hartree) to positive (blue, +0.58 hartree). Wavefunctions were calculated at the RHF/6-31+G** level and mapped on the 0.003 e/b^3 isodensity surfaces.

the C1′ carboxylate makes contacts with Lys22, Arg344, His385, and Arg386 (*5*, *6*).

Catalyzing Enolpyruvyl Activation. The pH dependence of acid-catalyzed EPSP hydrolysis indicated pK_a < −4 for C3′ (*22*). C3′ protonation will only occur if AroA exerts significant catalytic power to do so. Stabilization of such an unstable intermediate will not be accidental but rather a reflection of the intrinsic catalytic mechanism.

AroA-catalyzed EPSP hydrolysis is (1−5) × 10^3-fold faster than the nonenzymatic rate at pH 7, corresponding to 4−5 kcal/mol of transition state stabilization. The presence of P_i in the active site accelerates the normal reverse reaction a further 10^5-fold (*25*). Given the fact that the unactivated enolpyruvyl group does not react with nucleophiles, this rate acceleration indicates that P_i induces a change in the AroA active site to promote enolpyruvyl activation. This is consistent with conformational changes observed through Trp fluorescence. EPSP binding causes a decrease in Trp fluorescence, which has been correlated with closing down the active site (*11*, *23*). The same fluorescence decrease was observed with the D313A mutant (*25*), and titrating AroA_D313A·EPSP with P_i caused a further, large decrease in Trp fluorescence, evidence of a further conformational change.

Character of a Cationic Intermediate. If AroA is devoting catalytic power to stabilizing a cationic intermediate or transition state, that becomes a target motif for inhibitor design. Protonating C3′ changes the electrostatic potential surface of EPSP dramatically (Figure 6). The EPSP cation resembles the oxacarbenium ion intermediates (or oxacarbenium ion-like transition states) formed by glycosylases (*41*−*43*). Oxacarbenium ions are highly reactive electrophiles with almost no barrier to nucleophilic attack on the cationic carbon (*44*, *45*). By analogy to glycosyl oxacarbenium ions (e.g., see ref *43*), the EPSP cation will have significant C2′−O5 π-bonding, as well as some C2′−C3′ π-bonding resulting from hyperconjugation with the C3′−H3′ σ-bonds. The positive charge will reside predominantly on C2′. Like the EPSP cation, the *N*-acetylneuraminyl (sialic acid) oxacarbenium ion has a carboxyl group adjacent to the cationic center. It has a finite lifetime in solution, (1 to >3) × 10^{-11} s^{-1} (*46*, *47*), and computational studies indicate that the α-carboxylate group prefers a conformation perpendicular to the oxacarbenium ion, with no p-orbital overlap with the cationic carbon (*48*). This implies that carboxylate stabilizes the oxacarbenium ion inductively rather than through resonance stabilization. Glycosylases have long been targets of inhibitor design, and many cationic inhibitors that mimic the oxacarbenium ion have been characterized (*49*, *50*). This may provide a handle for designing AroA inhibitors.

ACKNOWLEDGMENT

We thank Fuzhong Zhang for invaluable advice in this study, Dr. Shehadeh Mizyed for preliminary experiments on EPSPK formation, Joan Lowe-Ching for help in characterizing acid-catalyzed EPSP hydrolysis, and Dr. Don Hughes for the NMR spectra of EPSPK.

SUPPORTING INFORMATION AVAILABLE

NMR spectra of EPSP ketal, shikimate 3-phosphate, and shikimic acid and a table of enzyme-bound intermediate species at $t = 1$ s, as determined by numerical simulation. This material is available free of charge via the Internet at http://pubs.acs.org.

REFERENCES

1. Anderson, K. S., and Johnson, K. A. (1990) Kinetic and structural analysis of enzyme intermediates: Lessons from EPSP synthase, *Chem. Rev. 90*, 1131−1149.
2. Roberts, F., Roberts, C. W., Johnson, J. J., Kyle, D. E., Krell, T., Coggins, J. R., Coombs, G. H., Milhous, W. K., Tzipori, S., Ferguson, D. J., Chakrabarti, D., and McLeod, R. (1998) Evidence for the shikimate pathway in apicomplexan parasites, *Nature 393*, 801−805.
3. Steinrucken, H. C., and Amrhein, N. (1980) The herbicide glyphosate is a potent inhibitor of 5-enolpyruvyl-shikimic acid-3-phosphate synthase, *Biochem. Biophys. Res. Commun. 94*, 1207−1212.
4. Kahan, F. M., Kahan, J. S., Cassidy, P. J., and Kropp, H. (1974) Mechanism of action of fosfomycin (phosphonomycin), *Ann. N.Y. Acad. Sci. 235*, 364−386.
5. Mizyed, S., Wright, J. E. I., Byczynski, B., and Berti, P. J. (2003) Identification of the catalytic residues of AroA (enolpyruvylshikimate 3-phosphate synthase) using partitioning analysis, *Biochemistry 42*, 6986−6995.
6. Eschenburg, S., Kabsch, W., Healy, M. L., and Schonbrunn, E. (2003) A new view of the mechanisms of UDP-*N*-acetylglucosamine enolpyruvyl transferase (MurA) and 5-enolpyruvylshikimate-3-phosphate synthase (AroA) derived from x-ray structures of their tetrahedral reaction intermediate states, *J. Biol. Chem. 278*, 49215−49222.
7. An, M., Maitra, U., Neidlein, U., and Bartlett, P. A. (2003) 5-Enolpyruvylshikimate 3-phosphate synthase: Chemical synthesis of the tetrahedral intermediate and assignment of the stereochem-

ical course of the enzymatic reaction, *J. Am. Chem. Soc. 125*, 12759−12767.
8. Anton, D. L., Hedstrom, L., Fish, S., and Abeles, R. H. (1983) Mechanism of enolpyruvylshikimate-3-phosphate synthase exchange of phosphoenolpyruvate with solvent protons, *Biochemistry 22*, 5903−5908.
9. Steinrucken, H. C., and Amrhein, N. (1984) 5-Enolpyruvylshikimate-3-phosphate synthase of *Klebsiella pneumoniae* 2. Inhibition by glyphosate [N-(phosphonomethyl)glycine], *Eur. J. Biochem. 143*, 351−357.
10. Boocock, M. R., and Coggins, J. R. (1983) Kinetics of 5-enolpyruvylshikimate-3-phosphate synthase inhibition by glyphosate, *FEBS Lett. 154*, 127−133.
11. Sammons, R. D., Gruys, K. J., Anderson, K. S., Johnson, K. A., and Sikorski, J. A. (1995) Reevaluating glyphosate as a transition-state inhibitor of EPSP synthase: identification of an EPSP synthase·EPSP·glyphosate ternary complex, *Biochemistry 34*, 6433−6440.
12. Leo, G. C., Sikorski, J. A., and Sammons, R. D. (1990) Novel product from EPSP synthase at equilibrium, *J. Am. Chem. Soc. 112*, 1653−1654.
13. Anderson, K. S., Sammons, R. D., Leo, G. C., Sikorski, J. A., Benesi, A. J., and Johnson, K. A. (1990) Observation by ^{13}C NMR of the EPSP synthase tetrahedral intermediate bound to the enzyme active site, *Biochemistry 29*, 1460−1465.
14. Barlow, P. N., Appleyard, R. J., Wilson, J. O., and Evans, J. N. (1989) Direct observation of the enzyme-intermediate complex of 5-enolpyruvylshikimate-3-phosphate synthase by ^{13}C NMR spectroscopy, *Biochemistry 28*, 7985−7991 [erratum: (1989) *Biochemistry 28*, 10093].
15. Studelska, D. R., McDowell, L. M., Espe, M. P., Klug, C. A., and Schaefer, J. (1997) Slowed enzymatic turnover allows characterization of intermediates by solid-state NMR, *Biochemistry 36*, 15555−15560.
16. Byczynski, B., Mizyed, S., and Berti, P. J. (2003) Nonenzymatic breakdown of the tetrahedral (α-carboxyketal phosphate) intermediates of MurA and AroA, two carboxyvinyl transferases. Protonation of different functional groups controls the rate and fate of breakdown, *J. Am. Chem. Soc. 125*, 12541−12550.
17. Kresge, A. J., Sagatys, D. S., and Chen, H. L. (1977) Vinyl ether hydrolysis. 9. Isotope effects on proton-transfer from hydronium ion, *J. Am. Chem. Soc. 99*, 7228−7233.
18. Kirby, A. J., and Williams, N. H. (1991) Efficient intramolecular general acid catalysis of vinyl ether hydrolysis by the neighboring carboxylic acid group, *J. Chem. Soc., Chem. Commun.*, 1643−1644.
19. Kirby, A. J., and Williams, N. H. (1991) There is no evidence for electrostatic catalysis of vinyl ether hydrolysis in water, *J. Chem. Soc., Chem. Commun.*, 1644−1645.
20. Loudon, G. M., Smith, C. K., and Zimmerman, S. E. (1974) Concurrent general acid-electrostatic catalysis in vinyl ether hydrolysis and aspartic-52 of lysozyme, *J. Am. Chem. Soc. 96*, 465−479.
21. Kresge, A. J. (1987) Unusual reactivity of prostacyclin—rational drug design through physical organic-chemistry, *Acc. Chem. Res. 20*, 364−370.
22. Kresge, A. J., Leibovitch, M., and Sikorski, J. A. (1992) Acid-catalyzed hydrolysis of 5-enolpyruvylshikimate 3-phosphate (EPSP) and some simple models of its vinyl ether functional group, *J. Am. Chem. Soc. 114*, 2618−2622.
23. Anderson, K. S., Sikorski, J. A., and Johnson, K. A. (1988) Evaluation of 5-enolpyruvoylshikimate-3-phosphate synthase substrate and inhibitor binding by stopped-flow and equilibrium fluorescence measurements, *Biochemistry 27*, 1604−1610.
24. Duggleby, R. G. (1983) Determination of the kinetic properties of enzymes catalysing coupled reaction sequences, *Biochim. Biophys. Acta 744*, 249−259.
25. Zhang, F., and Berti, P. J. (2006) Phosphate analogues as probes of the catalytic mechanisms of MurA and AroA, two carboxyvinyl transferases, *Biochemistry 45*, 6027−6037.
26. Anderson, K. S., Sikorski, J. A., and Johnson, K. A. (1988) A tetrahedral intermediate in the EPSP synthase reaction observed by rapid quench kinetics, *Biochemistry 27*, 7395−7406.
27. Anderson, K. S., and Johnson, K. A. (1990) "Kinetic competence" of the 5-enolpyruvoylshikimate-3-phosphate synthase tetrahedral intermediate, *J. Biol. Chem. 265*, 5567−5572.
28. Gruys, K. J., Walker, M. C., and Sikorski, J. A. (1992) Substrate synergism and the steady-state kinetic reaction mechanism for EPSP synthase from *Escherichia coli*, *Biochemistry 31*, 5534−5544.
29. Gruys, K. J., Marzabadi, M. R., Pansegrau, P. D., and Sikorski, J. A. (1993) Steady-state kinetic evaluation of the reverse reaction for *Escherichia coli* 5-enolpyruvoylshikimate-3-phosphate synthase, *Arch. Biochem. Biophys. 304*, 345−351.
30. Barshop, B. A., Wrenn, R. F., and Frieden, C. (1983) Analysis of numerical methods for computer simulation of kinetic processes: development of KINSIM—a flexible, portable system, *Anal. Biochem. 130*, 134−145.
31. Zimmerle, C. T., and Frieden, C. (1989) Analysis of progress curves by simulations generated by numerical integration, *Biochem. J. 258*, 381−387.
32. Cox, R. A., and Yates, K. (1978) Excess acidities—generalized method for determination of basicities in aqueous acid mixtures, *J. Am. Chem. Soc. 100*, 3861−3867.
33. Belarmino, A. T. N., Froehner, S., Zanette, D., Farah, J. P. S., Bunton, C. A., and Romsted, L. S. (2003) Effect of alkyl group size on the mechanism of acid hydrolyses of benzaldehyde acetals, *J. Org. Chem. 68*, 706−717.
34. Wiberg, K. B., and Squires, R. R. (1981) Thermochemical studies of carbonyl reactions. 2. Steric effects in acetal and ketal hydrolysis, *J. Am. Chem. Soc. 103*, 4473−4478.
35. Cleland, W. W. (1990) Kinetic competence of enzymic intermediates: fact or fiction?, *Biochemistry 29*, 3194−3197.
36. Charton, M. (1964) Definition of "inductive" substituent constants, *J. Org. Chem. 29*, 1222−1227.
37. Gelb, R. I. (1971) Conductometric determination of pK_a values. Oxalic and squaric acids, *Anal. Chem. 43*, 1110−1113.
38. Pinching, G. D., and Bates, R. G. (1948) Second dissociation constant of oxalic acid from 0° to 50° and the pH of certain oxalate buffer solutions, *J. Res. Natl. Bur. Stand. 40*, 405−416 (research paper no. 1885).
39. Ritchie, C. D. (1975) Cation-anion combination reactions. XIII. Correlation of the reactions of nucleophiles with esters, *J. Am. Chem. Soc. 97*, 1170−1179.
40. Schonbrunn, E., Eschenburg, S., Shuttleworth, W. E., Schloss, J. V., Amrhein, N., Evans, J. N. S., and Kabsch, W. (2001) Interaction of the herbicide glyphosate with its target enzyme 5-enolpyruvylshikimate 3-phosphate synthase in atomic detail, *Proc. Natl. Acad. Sci. U.S.A. 98*, 1376−1380.
41. Sinnott, M. L. (1990) Catalytic mechanisms of enzymic glycosyl transfer, *Chem. Rev. 90*, 1171−1202.
42. Zechel, D. L., and Withers, S. G. (2000) Glycosidase mechanisms: Anatomy of a finely tuned catalyst, *Acc. Chem. Res. 33*, 11−18.
43. Berti, P. J., and Tanaka, K. S. E. (2002) Transition state analysis using multiple kinetic isotope effects: Mechanisms of enzymatic and non-enzymatic glycoside hydrolysis and transfer, *Adv. Phys. Org. Chem. 37*, 239−314.
44. Richard, J. P., Williams, K. B., and Amyes, T. L. (1999) Intrinsic barriers for the reactions of an oxocarbenium ion in water, *J. Am. Chem. Soc. 121*, 8403−8404.
45. Richard, J. P. (1995) A consideration of the barrier for carbocation-nucleophile combination reactions, *Tetrahedron 51*, 1535−1573.
46. Knoll, T. L., and Bennet, A. J. (2004) Aqueous methanolysis of an alpha-D-N-acetylneuraminyl pyridinium zwitterion: solvolysis occurs with no intramolecular participation of the anomeric carboxylate group, *J. Phys. Org. Chem. 17*, 478−482.
47. Horenstein, B. A., and Bruner, M. (1998) The N-acetyl neuraminyl oxocarbenium ion is an intermediate in the presence of anionic nucleophiles, *J. Am. Chem. Soc. 120*, 1357−1362.
48. Horenstein, B. A. (1997) Quantum mechanical analysis of an alpha-carboxylate-substituted oxocarbenium ion. Isotope effects for formation of the sialyl cation and the origin of an unusually large secondary ^{14}C isotope effect, *J. Am. Chem. Soc. 119*, 1101−1107.
49. Bols, M. (1998) 1-Aza sugars, apparent transition state analogues of equatorial glycoside formation/cleavage, *Acc. Chem. Res. 31*, 1−8.
50. Lillelund, V. H., Jensen, H. H., Liang, X., and Bols, M. (2002) Recent developments of transition-state analogue glycosidase inhibitors of non-natural product origin, *Chem. Rev. 102*, 515−553.

BI0618316